Journal of Materials Chemistry C

Accepted Manuscript

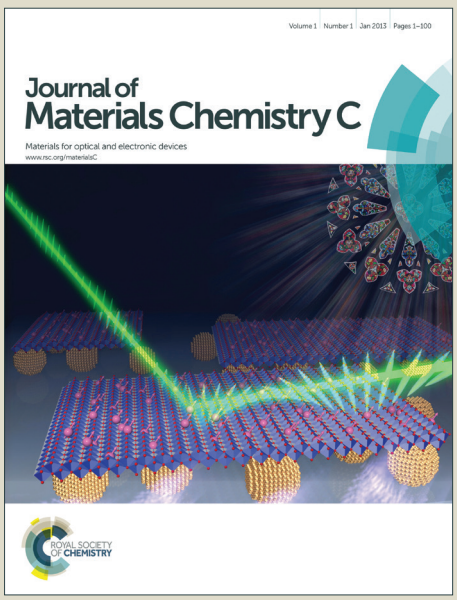

ROYAL SOCIETY OF CHEMISTRY

www.rsc.org/materialsC

ARTICLE TYPE www. rsc.org/xxxxxx | XXXXXXXX

Mixed interlayers at the interface between PEDOT:PSS and conjugated polymers provide charge transport control†

Adam J. Moulé,*[a] Min-Cherl Jung,[b] Chris W. Rochester,[a] Wolfgang Tress,[c] Daniela LaGrange,[a] Ian E. Jacobs,[a], Jun Li,[a] Scott A. Mauger,[a] M. Diego Rail,[d] Oliver Lin,[a] David J. Bilsky,[a] Yabing Qi,[b] Pieter Stroeve,[a] Louise A. Berben,[d] and Moritz Riede[e]

Received Xth XXXXXXXXXX 20XX, Accepted Xth XXXXXXXXX 20XX
First published on the web Xth XXXXXXXXXX 200X
DOI: 10.1039/b000000x

Poly(3,4-ethylenedioxythiophene)– poly(styrenesulphonate) (PEDOT:PSS) is the most used organic hole injecting or hole transporting material. The hole carrying matrix PEDOT is highly doped by the acidic dopant PSS. When coated onto a substrate, PEDOT:PSS makes a highly uniform conductive layer and a thin (<5 nm) overlayer of PSS covers the air interface. Semiconducting polymer layers for organic photovoltaics or light emitting diodes are coated on top. In this article, we demonstrate that the PSS layer will mix with almost all conjugated polymers upon thermal annealing. Depending on the Fermi energy of the polymer an electrochemical reaction can take place, p–type doping the polymer at the interface between the PEDOT:PSS and the semiconducting polymer. We use chemical and spectroscopic analysis to characterize the polymer / PSS interlayer. We show that the stable and insoluble interlayer has a large affect on the charge injection and extraction from the interface. Finally we demonstrate and electronically model organic photovoltaic devices are fabricated using these mixed interlayers.

1 Introduction

Over the last two decades, organic electronics such organic photovoltaic (OPV) and organic light emitting diodes (OLED) have evolved from laboratory curiosities to commercially viable devices. These devices consist of an organic semiconducting (OSC) layer sandwiched between two electrodes that are designed to create a directional current. For OPVs, one electrode is designed to selectively extract holes that are carried by the highest occupied molecular orbital (HOMO) of the OSC while the other electrode selectively extracts electrons from the lowest unoccupied molecular orbital (LUMO). These selective electrodes determine the direction of current in the device. A device with non–selective electrodes (low shunt resistance) has a high "dark" current and will perform inefficiently.[1,2] For OLED devices, one electrode selectively injects holes to the HOMO while the other electrode selectively injects electrons to the LUMO. Again in this case, the location (front or back) of the electrodes determines the direction of current flow and non–selective electrodes greatly limit the performance of the OLED device. The most common strategy to induce hole or electron selectivity in an electrode is to choose an electrode material with a Fermi energy that matches the HOMO or LUMO levels of the OSC, respectively.[1] In this case, no activation energy is required to inject or extract the charge from the electrode to the semiconductor. This is called an Ohmic contact because the resistance only depends on the material properties.[1]

To illustrate this idea, Fig. 1 refers to a simplified generic organic semiconductor under open circuit conditions with electrode materials designed for hole transport (left) and electron transport (right). For the hole contact electrode, an Ohmic contact occurs when the quasi–Fermi level for holes in the semiconductor has the same potential as the work function (ϕ) of the electrode (metal or doped semiconductor). This condition is considered ideal because no barrier exists for charge transport between the electrode and semiconductor HOMO. At the same time the LUMO states are depleted near the electrode (the quasi–Fermi level for electrons does not exist) so charge can only flow through the HOMO states.[3]

When the work function of the hole electrode (ϕ_H) is

† Electronic Supplementary Information (ESI) available: [details of any supplementary information available should be included here]. See DOI: 10.1039/b000000x/

[a] *Chemical Engineering and Materials Science Department, University of California, Davis, CA 95616, USA, Fax: +01 (530) 752-1013; Tel: +01 (530) 754-8669; E-mail: amoule@ucdavis.edu*
[b] *Energy Materials and Surface Sciences Unit, Okinawa Institute of Science and Technology Graduate University, 1919-1 Tancha Onna-son, Okinawa 904-0495 Japan*
[c] *Laboratory of Photonics and Interfaces, Swiss Federal Institute of Technology (EPFL), Station 6, Lausanne, CH 1015, Switzerland*
[d] *Department of Chemistry, University of California, Davis, CA 95616, USA*
[e] *Department of Physics, Oxford University, United Kingdom*

‡ Additional footnotes to the title and authors can be included *e.g.* 'Present address:' or 'These authors contributed equally to this work' as above using the symbols: ‡, §, and ¶. Please place the appropriate symbol next to the author's name and include a `\footnotetext` entry in the the correct place in the list.

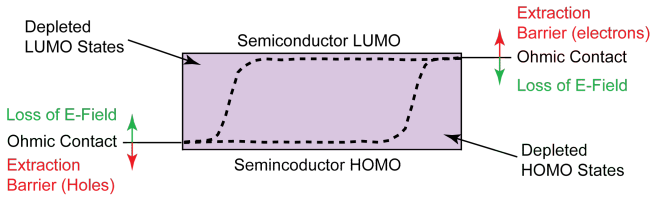

Fig. 1 Cartoon showing a generic organic semiconductor with quasi Fermi levels for holes and electrons marked as a dotted line. An Ohmic contact is achieved when the Φ of the electrode matches the quasi Fermi level of the semiconductor. An extraction barrier forms as the electrode Φ is raised/lowered into the LUMO/HOMO bands, while the applied electric field across the layer results is reduced as the Φ of the electrode moves into the band gap of the semiconductor.

larger than the quasi–Fermi level of the semiconductors HOMO ($E_F(HOMO)$), the difference in potential [$\Delta\phi = \phi_H - E_F(HOMO)$] is negative ($\phi$ is reported as a negative number) and a barrier exists for the extraction of holes from the semiconductor HOMO into the electrode. This extraction barrier can potentially be lowered by material changes such as doping or chemical reaction along the interface, band bending, or formation of a vacuum level shift.[4–8] Alternatively, $\Delta\phi$ could be positive, where ϕ_H lies within the band gap of the semiconductor. In this case, charges can exchange across the interface to compensate the potential difference, which leads to a loss in charge selectivity at the interface, increased dark current, and loss of electric field potential across the device layer. Loss of charge selectivity specifically means that charge can be injected or extracted from both the HOMO and LUMO bands of the semiconductor because when $\Delta\phi$ is positive, a quasi–Fermi level exists for both HOMO and LUMO states near the interface. Alternatively stated, the depletion zone is reduced so dark charge can flow.

At the electron extraction/injection electrode, an Ohmic contact occurs when the potential difference between the quasi–Fermi level of the LUMO ($E_F(LUMO)$) is equal to the work function of the electron collecting electrode (ϕ_N), i.e [$\Delta\phi_N = \phi_N - E_F(LUMO) = 0$]. At this electrode, a negative $\Delta\phi_N$ corresponds to the case of a loss of charge specificity and electric field loss across the device layer. Whereas a positive $\Delta\phi_N$ represents an injection or extraction barrier for electrons to and from the device layer. As for the hole electrode the injection/extraction barrier can potentially be lowered by material changes that result in, a vacuum level shift, band bending, doping, or chemical reaction at the interface (i.e. $\Delta\phi_N$ is lowered).[4–8]

Numerous organic[9–11] and inorganic[12] solution and vacuum processed materials have been developed for the specific purpose of affecting the charge transport through interfaces. The effects of changing a metal electrode[13,14] or semiconductor oxides[12] to affect hole and electron injecting/extracting are generally understood. Vacuum evaporated doped OSCs have also been well studied.[15] Fewer systematic studies[7] of solution processed doped organic electrodes have been published because organic materials tend to react or mix, which results in material specific changes at the interface. High levels of layer control using chemically tailored cross–linkable OSC materials using solution methods[16–18] have been demonstrated, but these materials are not widely available and are not doped.

Tress et. al. published a recent experiment/modeling study aimed at determining the electrical consequences of a $\Delta\phi$ across doped/undoped organic interfaces in a bi–layer OPV device.[19] For this study, the layers were deposited using evaporation of small molecules and co–evaporation of p– and n–type dopants, which made control of the $\Delta\phi$ across the interface relatively experimentally easy. The result of the study was to show that a $\Delta\phi$ across the interface caused a degradation of the device efficiency and formation of an "S–shaped" current density voltage (JV) curve.[19,20] The $\Delta\phi$ is compensated by charge transfer across the interface, creating a second diode in the opposite direction to the intended device.[20] When a forward bias is applied sufficient to overcome the $\Delta\phi$, normal diode behavior resumes.

As stated above, the model makes perfect sense. However, comparison to a different and widely used material combination; a solution coated bulk heterojunction (BHJ) OPV layer coated onto poly(3,4–ethylenedioxythiophene)–poly(styrenesulphonate) (PEDOT:PSS) the model appears to break down. OPV devices with high efficiency and no "S–shaped" JV curve are fabricated with a variety of polymers for which the $\Delta\phi$ is substantial (<0.5 V).[21] The purpose of this article is to explain the apparent break down of a very sensible model and to examine why this effect is masked in OPV devices containing PEDOT:PSS.

PEDOT:PSS has been the most widely used doped polymer material since its introduction in the late 90's.[22] Its popularity comes because of a combination of favorable characteristics including; transparency in the visible, high conductivity, stable work function, easy processibility, solubility in H_2O, and long shelf-life. PEDOT:PSS has been widely reported to be a hole selective charge transporter.[22,23] The components are reported to be mixed at a ratio of 1:6 PEDOT:PSS, with the PSS as dopant and PEDOT as the doped charge carrier.[23] X-ray photoelectron spectroscopy (XPS)[24–28] and (XAS)[29] of PEDOT:PSS surfaces reveals that the film surface is predominantly covered with PSS and with the sulphate group oriented toward the surface. Ellipsometric and conductivity measurements show that the PEDOT:PSS has an anisotropic structure with much higher conductivity in the plane of the substrate.[30,31] It was later found that the increased in–plane conductivity results from a particular film morphology of the PEDOT:PSS, which forms by collapse of micelles during drying.[32] These studies also confirmed a PSS skin on the PE-

DOT:PSS surface.[23,32,33]

The Moulé group has recently studied the interaction of PEDOT:PSS with neighboring layers in an attempt to explain the increased V_{oc} observed in OPV devices with PEDOT:PSS compared to devices fabricated with other electrode materials.[29] We found that the surface of the PEDOT:PSS was much richer in PSS than the bulk of the film (a result reported originally by Xing et. al.)[24] We also made two new significant observations. The first was that the PSS rich surface layer would mix with poly-3-hexylthiophene (P3HT) upon heating to above 150 °C.[29] Secondly, the two materials react to p–type dope the P3HT in the mixed layer with the mechanism:

2 HPSS + 2 P3HT $\rightarrow$ 2 P3HT^{+}PSS^{-} + H_2

In a follow up article, we showed that a bi–layer of P3HT with PEDOT:PSS had different conductive properties depending on the order of deposition because the PSS-rich layer is only in contact with the P3HT if the P3HT is deposited on top of the PEDOT:PSS. However if the PEDOT:PSS is coated onto the P3HT, even with heating to 200°C, there is no mixing or reaction between the materials because P3HT does not react with PEDOT:PSS, only with pure HPSS.[34] Given the directional dependence of the doping reaction with PEDOT:PSS, we hypothesize that the doping reaction dependents on the choice of OSC polymer and in particular on the polymer ionization energy. The following article demonstrates a generalized mechanism for interaction of PEDOT:PSS with various OSCs used in electronics applications. We discuss the heat induced mixing of various polymers with PEDOT:PSS at the PSS rich interface to form mixed interlayers. We also show significant electronic, chemical, and structural characterization of the mixed interlayer. Finally we demonstrate that OPV devices with prepared interlayers of the other semiconducting polymers and show that the current denisty/voltage (JV) behavior is predictable based on the Tress model for charge injection and extraction.

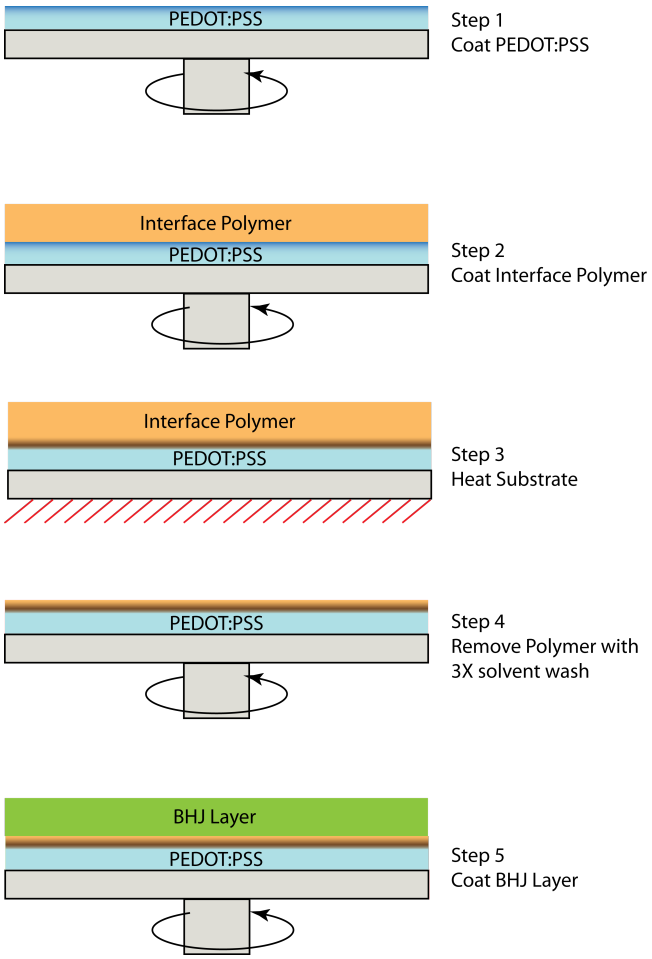

Fig. 2 Cartoon shows the fabrication steps used to prepare polymer interlayers between PEDOT:PSS and the BHJ layer. The figure is color coded as follows: the substrate is gray, the PEDOT:PSS layer is blue, the interface polymer is orange, the mixed PSS/interface polymer is brown and the BHJ layer is green.

2 Experimental

Polymer interlayers were deposited between the PEDOT:PSS layer and active OPV layer using the following steps (Fig. 2). First, the PEDOT:PSS layer itself is spin coated onto a cleaned indium tin oxide ITO substrate at 2500 rpm yielding a layer with ~40 nm thickness. In Fig. 2 the PEDOT is demarked as blue while the PSS, which segregates to the surface, is marked in dark blue. Next the interlayer polymer (orange in fig. 2) is spin coated onto the PEDOT:PSS substrate. The thickness of this interlayer polymer does not matter, so typically only 30–40 nm of polymer is coated. The third step is to heat the layer stack to induce mixing and/or reaction between the PSS and the interlayer polymer with the mixed polymer marked in brown. Fourth, the excess interlayer polymer is removed using a good solvent for the polymer such as chlorobenzene, chloroform or toluene by spin coating several times on to the completed interlayer. Finally, a BHJ polymer/fullerene mixture is coated onto the interlayer.

X-ray reflectometry (XRR) samples were coated onto Si/SiO_2 substrates and heated to 110 °C to remove excess water. The heated sample was further heated to 150 °C. Samples were stored under nitrogen to prevent rehydration of the film. XRR was performed at beam line 2–1 at the Stanford Synchrotron Radiation Lightsource (SSRL).

The H_2 capture test was performed with mixtures of PSS and P3HT, APFO–3 and F8BT. In each case the polymer was mechanically mixed with PSS and placed into a sealed glass vial. The sample was heated to 180 °C for 30 minutes and then the seal was broken with a syringe. Several μl of gas was extracted from the vial and injected into a GCMS spectrome-

ter. The ratio of H_2 to O_2 was used to determine if H_2 was off gassed during heating.

Contact angle data were taken on substrates that were prepared as described above. The initial contact angle of a water droplet was measured using a Goniometer and microscope camera. These initial data were taken within 30–50 s of water contact. For longer times the PEDOT:PSS layer can swell considerably and the contact angle will be reduced and the interlayer no longer determines the contact angle.

UV/vis and Fluorescence spectra were taken on a Perkin Elmer 770C UV/vis/NIR and Varian Cary Fluorescence spectrometer, respectively. The solution state spectra were taken at low (5 mg/ml) concentrations. Film spectra were taken on films cast on glass with a thickness of ∼80 nm. P3HT and Poly[(9,9-di-n-octylfluorenyl-2,7-diyl)-alt-(benzo[2,1,3]thiadiazol-4,8-diyl)] (F8BT) were purchased from Sigma. Poly[(9,9-dioctylfluorenyl-2,7-diyl)-alt-5,5-(4,7-di-2-thienyl-2,1,3-benzothiadiazole)] (APFO–3) was generously donated by the groups of U. Scherf at The University of Wuppertal, Germany and O. Ingan as at Linköping University, Sweden.

Cyclic voltammograms (CVs) were recorded under a nitrogen (Praxair, 99.998%) atmosphere using a CH Instruments Electrochemical Analyzer Model 620D or 1100, a glassy carbon working electrode (CH Instruments, nominal surface area of 0.0707 cm^2), a platinum wire auxiliary electrode, and a $Ag/AgNO_3$ (0.001M) non-aqueous reference electrode with a Vycor tip. Reported potentials were all referenced to the SCE couple, and were determined using ferrocene as an internal standard where $E_{1/2}$ ferrocene/ferrocenium is +0.40 V v. SCE in acetonitrile. Non-aqueous electrolyte solutions were stored over 3 *Å* molecular sieves which had been activated by heating under vacuum at 200°C for at least 72 hours. All other reagents were purchased from commercial vendors and used as received.

OPV devices were prepared using BHJ solution of 3:2 P3HT:[6,6]-phenyl-C61-butyric acid methyl ester (PCBM) at a concentration of 20 mg/ml in a solvent mixture of 97 v% chlorobenzene (CLB) and 3 v% nitrobenzene (NB). This solvent mixture was chosen because it creates a high FF and PCE morphology for P3HT/PCBM devices with no annealing needed.[35] The spinning speed was adjusted to coat BHJ layers of ∼ 80 nm. The coating speed had to be adjusted because the surface energy of the substrate layer changes due to the presence of an interlayer. Variation of the current denisty at negative bias in devices is due to small variations in BHJ layer thickness. A Ca/Ag electrode with thicknesses 5 nm/150 nm was evaporated on top of the BHJ layer through a shadow mask. Devices were measured at ∼ 0.4 suns power using a solar simulator from Radiant Source Technology and a Keitheley 2420 source measurement unit.

XPS and UPS samples were prepared at UC Davis as described in section 2 and transported to Okinawa Institute of Technology and Science in a sealed container back-filled with dry N_2 gas. For the measurements of ultra-violet and x-ray photoelectron spectroscopy (UPS and XPS), we used the He I line (21.2 eV) from a discharge lamp, unmonochromated Mg$K\alpha$ (1253.6 eV) and EA125 energy analyzer with single channeltron that were made by Focus and Omicron Nanotechnology. The energy resolution is 0.15 eV for UPS and 0.7 eV for XPS. The Fermi edge of gold deposited on a high n-doped Si substrate (0.011 – 0.015 Ω·cm) was used to determine the Fermi energy position and the instrumental resolution. The chemical states of polymer samples were obtained with C 1*s*, O 1*s*, N 1*s* and S 2*p* core-level spectrum. The binding energies were calibrated with reference to the Au $4f_{7/2}$ level (84.0 eV).[42] The base, UPS and XPS working pressures of analysis chamber were 1.0×10^{-10}, 2.0×10^{-8} and 5.0×10^{-10} Torr, respectively.

3 Results and discussion

3.1 Vertical Segregation of PEDOT:PSS

We previously performed x-ray reflectometry (XRR) of PEDOT:PSS.[34] We now compare with PEDOT:PSS after annealing to 150 °C and in both cases found that the thickness and density of the PSS at the surface could be calculated. Fig. 3 shows the PSS weight fraction vs. depth determined using XRR and with $x = 0$ defined as the interface between the PEDOT:PSS layer and the Si/SiO_2 substrate. With heating the film shrinks by ∼5 Å due to loss of PSS content, as seen in the decrease in the weight fraction for the bulk. At the air interface a 30 Å layer of pure PSS forms upon coating. This PSS surface layer becomes slightly thicker and more pure with heating in air.

3.2 Determination of Mixing between polymers and PSS

3.2.1 Contact angle measurements An important question in this work is to determine if, or at which temperature, common conjugated polymers used for OPV BHJ layers or OLED emission layers will mix with or react with the p–type dopant PSS. As shown in Fig. 3 the substrate is covered with a thin skin of PSS, which is an acid, and therefore is highly hydrophilic. Fig. 4 shows the contact angle for a water droplet vs. heat treatment temperature for interlayer samples of P3HT, APFO–3, and F8BT that were prepared as shown in Fig. 2. Contact angles and surface coverage for other electronic polymers are shown in the supplementary information Fig. SA1. For PEDOT:PSS with no interlayer, it can be seen that the contact angle is between 7° and 15° under all annealing conditions, which indicates a strong favorable interaction with water. Contact angle measurements of the pure polymers are in-

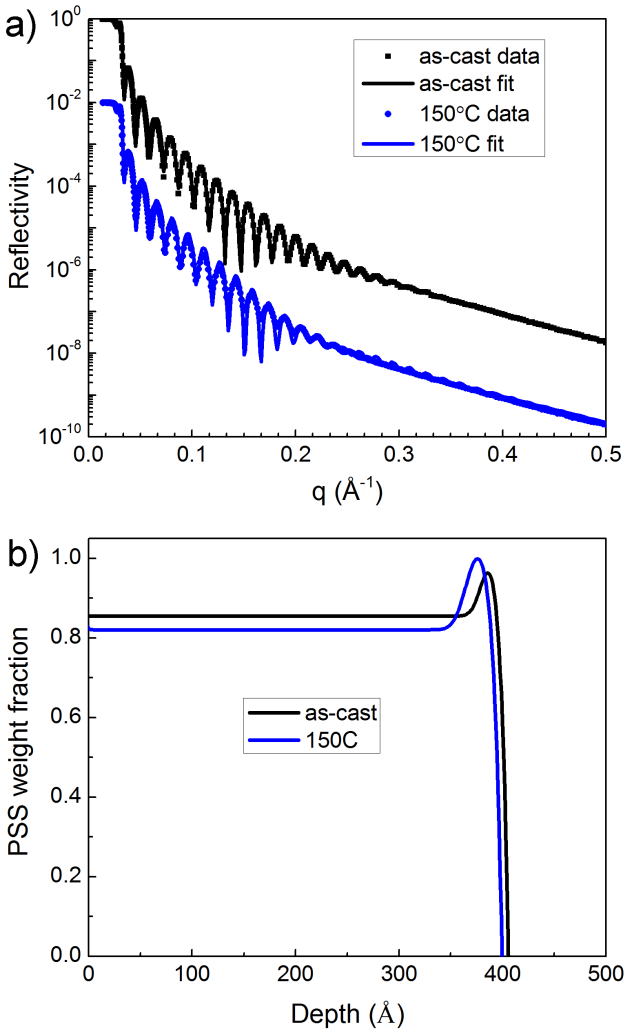

Fig. 3 a) X-ray reflectometry data and modeled fit for PEDOT:PSS on an Si/SiO_2 substrate before and after heating to 150 °C. b) shows the PSS weight fraction vs. depth in the layer with x = 0 defined as the interface between PEDOT:PSS and Si/SiO_2. The PSS rich layer occupies the top 3-5 nm and heating increases the vertical segregation of PSS.

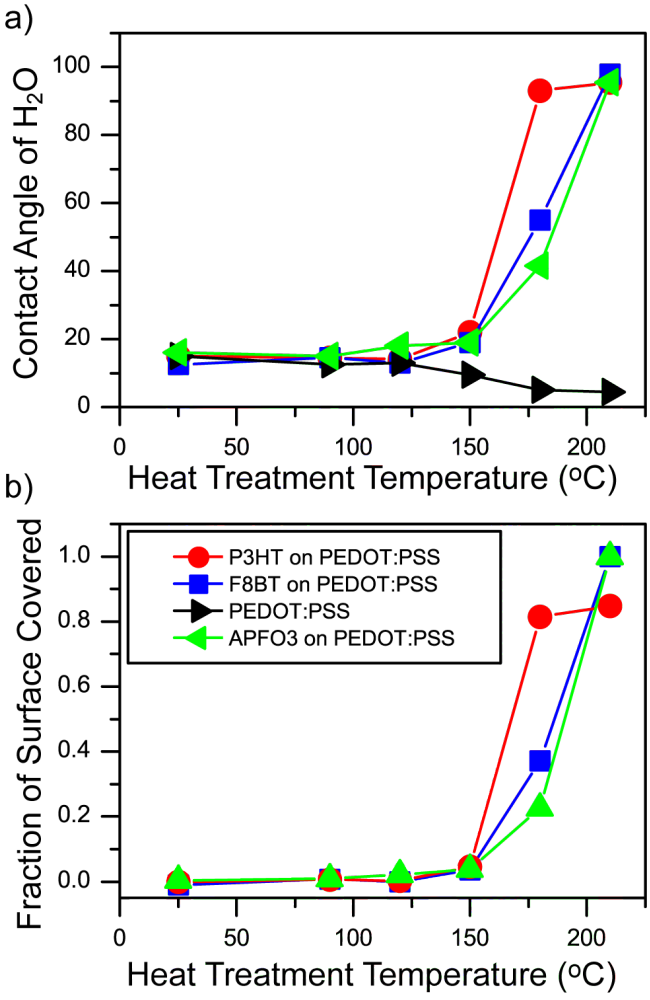

Fig. 4 a) Contact angle vs heat treatment temperature for PEDOT:PSS surfaces that were pre–treated as described in section 2 with various polymers. b) Calculated surface fraction coverage of the interlayer polymer vs. annealing temperature.

dicated as dashed lines and all occur with a contact angle of over 90° indicating strong hydrophobicity. For samples prepared as indicated in Fig. 2, the heating step will either induce mixing/reaction between the PSS and interlayer polymer or not. To quantify the presence of interlayer polymer remaining at the surface, the fraction f of the surface covered by interlayer polymer on the washed samples was calculated at each temperature T using the Cassie–Baxter equation[36],

$$\cos\theta_c = f\cos\theta_{\text{Interlayer}} + (1-f)\cos\theta_{\text{PEDOT:PSS}}, \qquad (1)$$

where $\theta_{\text{Interlayer}}$ and $\theta_{\text{PEDOT:PSS}}$ are the measured contact angles of water on the pure interlayer polymer and PEDOT:PSS respectively (assuming that $\theta_{\text{Interlayer}}$ is the same at all temperatures). At temperatures between 120 °C and 210 °C all of the polymers tested except PCPDTBT (see supporting information Fig. S1) mix/react with the PEDOT:PSS surface and show a surface coverage of over 80%. We assume that PCPDTBT does not mix with PSS because it is composed of two different bulky multi-cyclic aromatic groups and that it would mix with PSS at higher temperatures. However since PEDOT:PSS breaks down at higher temperatures,[37] we did not extend our study beyond 210 °C. We also tested whether the fullerene acceptor PCBM mixes/reacts with the PEDOT:PSS surface. Contact angle results (supplementary information Fig. S1)

show that no PCBM can be detected at the surface. However, Lu et al. reported PCBM intrusion into the PEDOT:PSS measured using another technique.[38] Contact angle measurements are a simple and accurate method to determine surface coverage of hydrophobic polymers on a hydrophylic substrate. These results show that we can use the procedure shown in Fig. 2 to prepare a complete layer of most conjugated polymers onto PEDOT:PSS using only annealing and dissolution steps.

3.2.2 X-ray photoelectron spectroscopy In order to learn more about the composition of the interlayer, we used x-ray photoelectron spectroscopy (XPS) to study the exposed surface of washed interlayers, prepared as shown in Fig. 2 with a 180 °C annealing temperature. Fig. 5 shows XPS spectra corresponding to the S 2*p* spectral region for several polymers. The black lines correspond to neat polymers of P3HT (left), APFO–3 (middle) and F8BT (right) coated onto ITO. Also displayed are samples of PEDOT:PSS on ITO with interlayers of each polymers coated on top P3HT (red–dashed), APFO-3 (green–dashed) and F8BT (blue–dashed). The contact angle measurements show us that some polymer material remains on the PEDOT:PSS surface. Here we use XPS to determine the composition of the interlayer. XPS is a powerful tool to understand chemical states of polymer thin–film to depths of 4–6 nm.[39]

In order to analyze the XPS spectra in more detail, we fitted S 2*p* core-level spectrum using Doniach-Sŭnjić curves convoluted with Gaussian distribution of 0.5 eV full-width at half maximum.[40] The background due to inelastic scattering was subtracted by the Shirley (or integral) method.[41] The fitting results are shown in supporting information Fig. S2. Analyzing the P3HT sample, a group of two peaks with different intensities can be identified with the stronger peak at the binding energy of 163.3 eV. These two peaks can be assigned to be the spin-orbit split $2p_{3/2}$ and $2p_{1/2}$ of S^{II}, which is originated from P3HT. For fitting the S 2*p* the intensity ratio of spin–orbit splitting used was 1:2 for the $p_{1/2}$:$p_{3/2}$. For the P3HT/PEDOT:PSS/ITO sample, two groups of peaks in the S 2*p* region can be identified. The first group contains two peaks with the same binding energies as those in the P3HT/ITO sample. These two peaks can be assigned to be the spin-orbit split $2p_{3/2}$ and $2p_{1/2}$ of S^{II}, which is originated from P3HT and PEDOT. The second group also contains two peaks with different intensities. The stronger peak is located at a binding energy of 167.2 eV. These two peaks can be assigned to be the spin–orbit split $2p_{3/2}$ and $2p_{1/2}$ of S^{VI}, which originates from PSS. Comparing the two spectra, the black line is P3HT only and the red line is mixed P3HT:PSS (see fit in supporting information Fig S2). The spectra can be interpreted to show that P3HT and PSS are detected in the 4 nm closest to the surface with a ratio of 6.5:1.

Examining the other S 2*p* spectra, for the APFO-3/ITO sample a group of two peaks with different intensities can be identified with the stronger peak at the binding energy of 163.6 eV. These two peaks can be assigned to be the $2p_{3/2}$ and $2p_{1/2}$ of S^{II}, which originates from APFO-3. For the F8BT/ITO sample, a group of two peaks with different intensities can be identified with the stronger peak at the binding energy of 164.8 eV. These two peaks can be assigned to $2p_{3/2}$ and $2p_{1/2}$ of S^{II}, which originates from F8BT. The intensity ratio of the splitting *p* is 2:1 in $2p_{3/2}$ and $2p_{1/2}$ (See supporting information Fig. S2).[42] As above, the strong peak located at 167.2 eV is associated with the Sulfur on PSS. For both F8BT and APFO-3, the peak intensities of the third group is significantly stronger than those of the second group, suggesting that the surface is PSS rich.[43] The F8BT data was fit to find a 3:2 ratio of PEDOT:PSS to F8BT in the 4 nm closest to the sample surface after heating at 180 °C and washing with CB. The APFO-3 data is noisy and so could not be fit, but the ratio is qualitatively similar to that of F8BT/PSS. By comparison, the P3HT XPS sample had a larger amount of P3HT remaining after washing, indicating a mixed layer that is richer in P3HT. This result is expected based on the contact angle results presented in Fig. 4. P3HT mixes with PSS at a lower temperature than either F8BT of APFO-3.

XPS spectra were also taken at the C 1*s* and O 1*s* energy loss ranges (supporting information Fig. S3). The C 1*s* spectra show very little change in each case, indicating that the sample surface remains carbon rich (not a surprise). The O 1*s* spectra are more diagnostic. Since P3HT, APFO-3, and F8BT do not have any oxygen in their structure, detection of oxygen has to come from either the C–O–C bonds on the PEDOT or the SO_3 groups from the PSS. The O 1*s* spectra are all characteristic of the signal from the SO_3 groups on the PSS of PEDOT:PSS. Again the XPS data confirms that the top 4 nm of the interlayer is composed of a mixture of polymer with PSS.[39]

3.3 Reaction Mechanism

In a previous publication, we studied the annealing dependent interaction between PEDOT:PSS and P3HT.[29] A series of tests were used to show that P3HT reacts with PSS upon heating to above 150 °C to form p–type doped P3HT and the reaction product H_2.[29] We hypothesized that P3HT is doped by PSS due to the low ionization energy of P3HT (4.7 eV) compared to the work function (Φ) of PEDOT:PSS (5.1 eV). We also hypothesized that the reaction is limited to those P3HT strands that mix intimately with PSS, meaning that the reaction can only occur at the interface between the materials. In the absence of mixing this reaction is not possible. We now note that another hypothesized reaction with PSS has been published.[44] The Meerholz group showed that the PSS can catalyze a ring-opening reaction on oxetane cross-linking

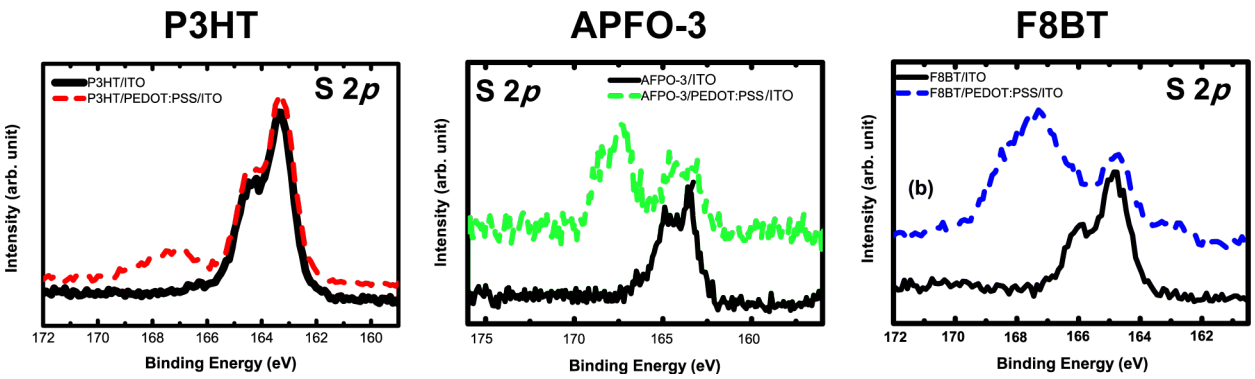

Fig. 5 Sulfur L–edge x–ray photoelectron spectroscopy of a) P3HT on ITO and ITO/PEDOT:PSS substrates, b) APFO–3 on ITO and ITO/PEDOT:PSS substrates, and c) F8BT on ITO and ITO/PEDOT:PSS substrates.

groups. In this case, excess protons from the PSS are carried through the organic layer with the HSO_3^- or SO_4^{-2} providing charge balance. We do not believe that proton transfer is active in the reaction reported here because the thickness of the mixed interlayer does not increase with increasing heat treatment time as is the case for the reaction reported by Meerholz.

APFO–3 and F8BT both have much higher ionization energies than P3HT. We tested whether the heated mixture of PSS with each of these polymers would produce H_2 and found that we were unable to detect an H_2 product. This rather easy and crude test indicates that APFO–3 and F8BT are not oxidized by PSS. However, since the CA results showed that these polymers will mix with PSS upon heating and XPS shows that some polymer remains on the surface, it is also possible that the H_2 is below the detection limit of the gas chromotograph mass spectrometer (GCMS). For this reason we conduct analysis using CV, optical measurements, and UPS. Because this research community is composed of chemists, physicists, and engineers with differing tools, CV and UPS data were both taken and compared. UPS provides more accurate data but is more costly and requires much more expertise. The CV data gives a reasonable estimate of the HOMO and LUMO onset energies. Comparison of the data give an idea of the likely error bars on the CV data.

3.4 Detecting a reaction at an internal interface

3.4.1 Cyclic Voltammetry CV measurements were made of neat polymers in a 1:1 mixture of 1,2 dichlorobenzene and methylene chloride with ferocene as the reference. The first oxidation and first reduction potentials of the polymer (E_{ox} and E_{red}) are listed in Table 1. The Φ of PEDOT:PSS has been measured using UPS or Kelvin force probe set the Fermi energy of PEDOT:PSS to 5.1-5.3 V below vacuum.[29,33,45] This reference is a generally agreed upon Fermi energy of PEDOT:PSS. In addition, the oxidation potential E_{ox} of a PEDOT:PSS film was measured using CV.[46] We assume that E_{ox} of PEDOT:PSS measured using CV is equivalent to Φ measured using UPS and equate a linear scale between CV and UPS with PEDOT:PSS as the reference point. All other electrochemical states measured using CV from other polymers are referenced to this.[33,47] In the fifth row, the polymer band gap (E_{gap}(CV)) determined from taking the difference between E_{ox} and E_{red} is listed. Note that the reduction potential cannot be measured reversibly using CV, so the E_{red} and E*gap*(CV) will both be over estimated by this measurement.

A CV measurement does not measure the Fermi energy of the polymer but does allow us to compare several polymers under identical electrochemical conditions. Assuming that no charge movement occurs (the non-contact case) we can estimate the over potential required to inject or extract charge from the PEDOT:PSS electrode (E_Δ). This is the equivalent of assuming that the PEDOT:PSS oxidation potential sets the work function for the substrate and we are estimating the extraction potential from the HOMO level of the polymer. In this case, P3HT has a 0.4 V extraction barrier for a hole from PEDOT:PSS (equivalent to 0.4 V injection potential for an electron). By comparison, APFO–3 and F8BT have 0.35 V and 0.58 V, respectively, over potential to extract holes from PEDOT:PSS. This simple analysis shows that from CV measurements, an extraction barrier for holes is expected for P3HT on PEDOT:PSS while hole extraction is favored for APFO–3 and F8BT. Many assumptions were made to obtain these estimates. We will next use UPS to measure the Fermi energy directly and compare to the CV estimates here.

3.4.2 Optical Measurements For comparison we measured the absorption spectra of each polymer in both a fully dissolved sample, which compares well to the CV measurement and a film sample, which compares well to a UPS sample. These spectra are in supporting information Fig. S3 and have been published in multiple other articles.[21,48,49] In each case the optical band gap E_{gap} for both samples is listed in

Table 1. In general, E_{gap} is lower for film samples because the exciton state energy is lowered by delocalization across multiple polymer chains in a solid sample.[50]

3.4.3 Ultraviolet Photoelectron Spectroscopy We now analyze UPS spectra of PEDOT:PSS/polymer bi–layers that were prepared by annealing at a PEDOT:PSS/polymer bi–layer at 180°C. This sample shows the effect of bi–layer formation on the top surface of the polymer layer. Fig. 6a shows UPS He I spectra of ITO (black) and PEDOT:PSS/ITO (gray–dashed) samples prepared with identical heating steps to the other samples. The work function is determined by measuring the secondary electron cutoff shown on the left side of the figure. Work function values are determined to be 3.6 eV and 4.6 eV for ITO and PEDOT:PSS/ITO, respectively. Both values are lower than reported elsewhere,[43] which is possibly caused by ambient exposure.[51]

Fig. 6b shows UPS He I spectra of P3HT/ITO (black) and P3HT/PEDOT:PSS/ITO (red–dashed) samples. The ϕ for the P3HT/ITO sample is is 3.5 eV. The leading edge of the HOMO features is 1.1 eV below the Fermi level. Thus, the ionization energy is 4.6 eV, which is consistent with the literature value and with both CV measurements above.[47,52] Based on the HOMO–LUMO optical gap value of 1.9 eV for P3HT, the Fermi level is just slightly below the middle of the HOMO–LUMO gap. The roughly mid-gap position of the Fermi level is in good agreement with the fact that the P3HT layer in this sample is mainly intrinsic. In addition, the work function of P3HT/ITO is only 0.1 eV lower than that of the bare ITO substrate, which indicates only weak charge transfer occurs at the P3HT/ITO interface. On the other hand, when an interface layer of P3HT/PEDOT:PSS is formed on ITO, the whole spectrum shifts towards lower binding energies. The Fermi levels shift towards the HOMO edge by approximately 0.7 eV, which is schematically illustrated in Fig. 7. Taking into account such a shift, the difference between the Fermi level and HOMO level is 0.4 eV, exactly the same energy as determined from CV as the over potential required to inject holes into PEDOT:PSS. The significant shift of the Fermi level towards a position just 0.4 eV higher than the HOMO level is likely caused by the p-type doping of P3HT by PEDOT:PSS. This p-type doping reaction removes the over potential required to injection holes from P3HT to PEDOT:PSS. Such a strong p-type doping behavior also implies that the electron affinity (EA) of PEDOT:PSS is larger than or close to 4.6 eV.

Fig. 6b shows UPS He I spectra of APFO–3/ITO (black) and APFO–3/PEDOT:PSS/ITO (green–dashed) samples. The work function is 2.9 eV for the APFO–3/ITO sample. The leading edge of the HOMO features is 2.44 eV below the Fermi level and so 5.34 eV which is a smaller ionization energy than other published data. Previously published IE was 5.8 eV.[53] These measurements indicate that the Fermi energy is within or very close to the LUMO band. This result is inconsistent with a typical understanding of how organic semiconductors operate and is thus most likely a measurement artifact. Perhaps the sample was exposed to oxygen before measurement. The ϕ_N of APFO–3/ITO is significantly larger (by 0.7 eV) than that of the bare ITO substrate, which indicates substantial electron transfer from APFO–3 to ITO at the APFO–3/ITO interface. When a mixed interface layer of APFO–3/PEDOT:PSS is formed on ITO, the Fermi level shifts strongly away from the LUMO band and is now roughly evenly between the HOMO and LUMO levels, which is schematically illustrated in Fig. 7. This result is consistent with the earlier report of ambipolar transport in APFO–3 and is also consistent with previously published OPV results.[54,55] We conclude that the APFO–3/ITO sample is an artifact. The Fermi energy in the APFO/PEDOT:PSS/ITO sample is 1.1 eV higher than the HOMO level, which suggests an absence of the p–doping effect, in contrast to what was found with the P3HT/PEDOT:PSS sample.

Fig. 6c shows UPS He I spectra of F8BT/ITO (black) and F8BT/PEDOT:PSS/ITO (blue–dashed) samples. The work function is 4.6 eV for the F8BT/ITO sample. The leading edge of the HOMO features is 1.8 eV below the Fermi level. Thus, the ionization energy is 6.4 eV, which is 0.5 eV larger than the reported literature value.[56] Based on the HOMO-LUMO gap value of 2.3 eV for F8BT, the Fermi level is roughly at the middle position of the HOMO-LUMO gap but closer to the LUMO. The ϕ_N of F8BT/ITO is significantly larger (by 1.0 eV) than that of the bare ITO substrate, which indicates substantial electron transfer from ITO to F8BT at the F8BT/ITO interface. Such charge transfer is likely the cause for the shifting of the Fermi level in F8BT closer to the LUMO. When a mixed interface layer of F8BT/PEDOT:PSS is formed on ITO, the Fermi level shifts slightly away from the HOMO edge by approximately 0.2 eV, which is schematically illustrated in Fig. 7. The Fermi level in the F8BT/PEDOT:PSS/ITO is 2.0 eV higher than the HOMO, which suggests an absence of the p-doping effect. This observation is in sharp contrast with what was found on the P3HT/PEDOT:PSS sample.

All measured CV, UPS, and optical data including the change in Fermi Energy (ΔE_F) are listed in Table 1. In addition we list the results of the H_2 capture test.[29] Table 1 lists the first oxidation potentials (E_{ox}) for the interlayer polymers as determined by CV. In the third row, E_{ox} is converted to ionization energy (IE) by comparison with literature ultraviolet photoelectron spectroscopy (UPS) of PEDOT:PSS.[29] with reported Φ for of -5.1 eV. With no other information we can expect that polymers with IE lesser than 5.1 eV might favorably donate electrons to PEDOT:PSS, as was shown for P3HT. However, a recent article by Greiner et. al. showed that conjugated organic molecules donate electrons to oxide substrates if the positive polaron state of the absorbed molecule lies closer

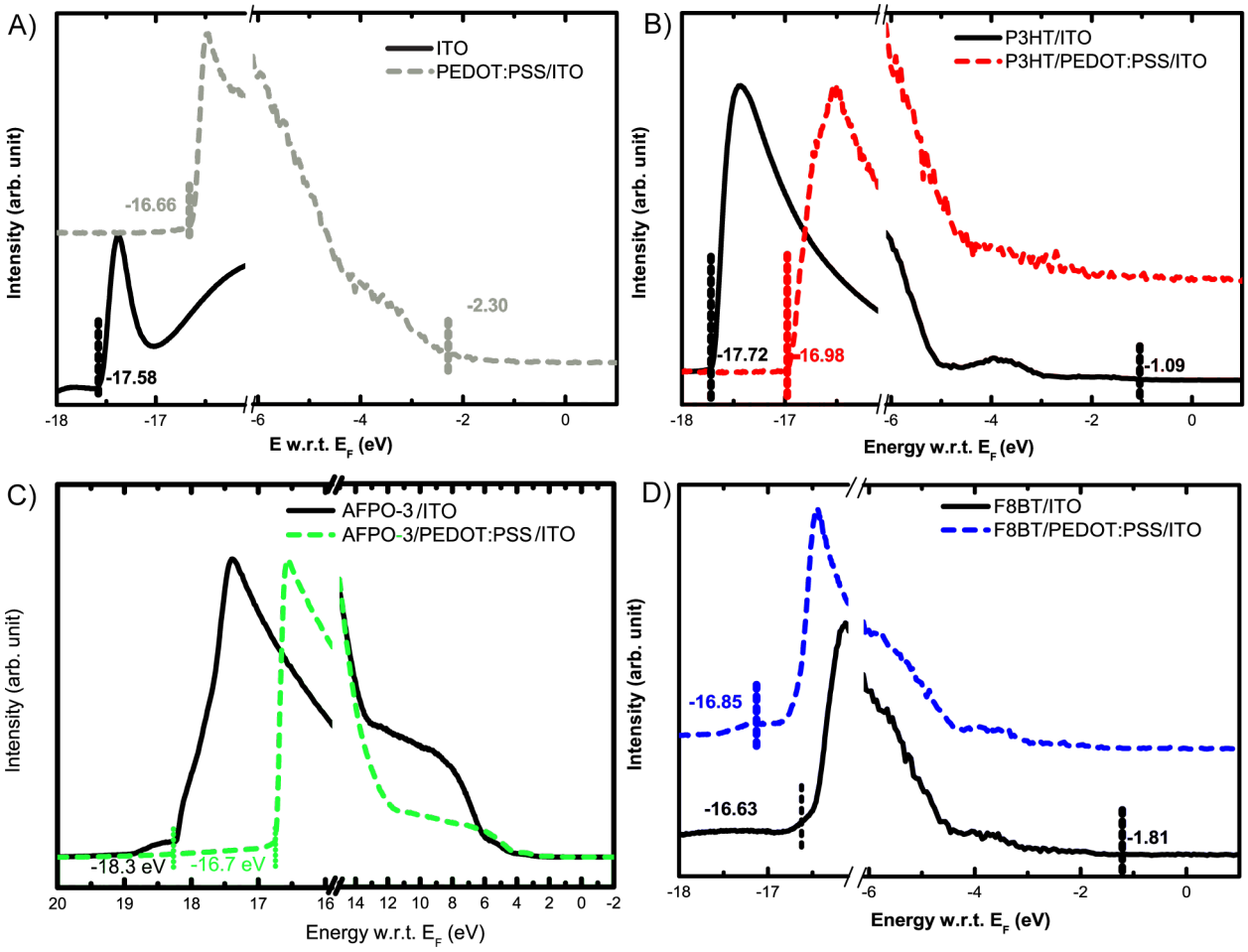

Fig. 6 Ultraviolet photoelectron spectroscopy of A) PEDOT:PSS on ITO, B) P3HT on PEDOT:PSS and ITO, and C) F8BT on PEDOT:PSS and ITO).

to the vacuum level than the Fermi energy of the substrate.[57] We compare data taken from CV, optical measurements, and UPS to measure the energy gap between the ionization energy (also top of HOMO band) of the polymer and the polaron level of the polymers on PEDOT:PSS. This table establishes that CV measurements give an rough estimate of the energy level allignment between polymers, but that interfacial states between PEDOT:PSS and polymers can change the Fermi level allignment, radically changing the hole extraction potential between the polymer and the PEDOT:PSS. This change is due to doping of the polymer by PSS. Only P3HT is p–type doped by PSS while APFO–3 and F8BT are not p–type doped by PSS.

3.5 Interlayers in Devices

The above sections have established how large the energy barrier for charge injection/extraction should be between PEDOT:PSS and a variety of donor polymers used for OPV and OLEDs. It is clear in each case that PEDOT:PSS would be the hole collecting/injection electrode with a low work function metal collecting/injection electrons at the other interface. However, it is also clear that only some polymers (with a smaller IE than the fermi energy (E_f) of PEDOT:PSS) are p-type doped from the PSS, while others do not react with PSS. From the cases shown above, P3HT is doped by PEDOT:PSS while APFO–3 and F8BT are not because they have higher Fermi energies.

The next step is to establish how the mixed interface layer will affect the electronic function of an OPV device. In a typical BHJ fabrication, the mixture is coated onto the PEDOT:PSS and later the device may or may not be heated. If heating with sufficient temperature occurs, the polymer in the BHJ will mix with the PSS but fullerene will not (see Fig. 4). These processes occur for every heated BHJ device. For this study, we add the additional step that we can prepare a mixed

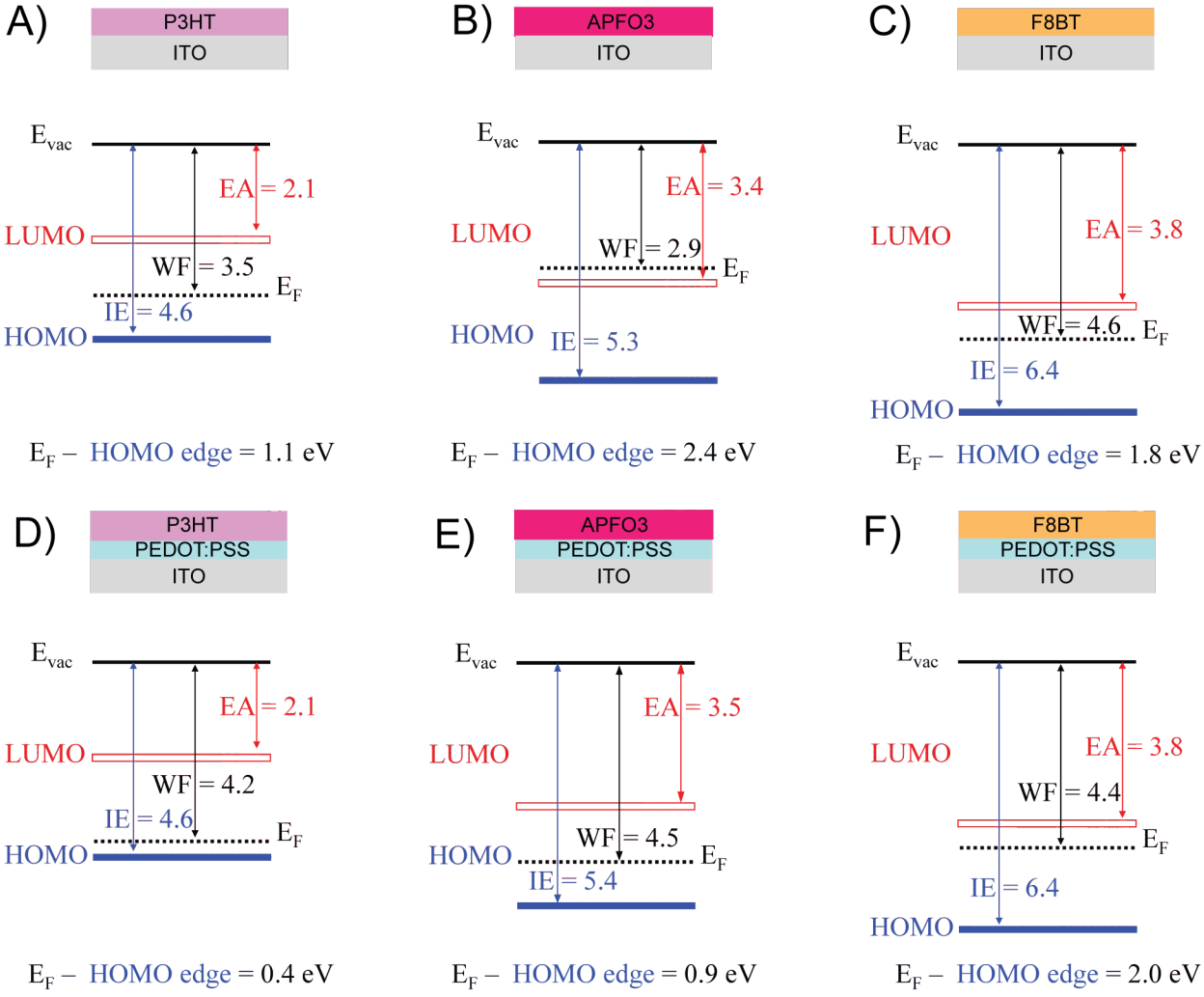

Fig. 7 Energy level diagrams showing the results of UPS for P3HT, APFO–3 and F8BT on an ITO substrate, a), b) and c) respectively. d), e) and f) are corresponding diagrams derived from UPS of P3HT, APFO–3 and F8BT coated onto ITO/PEDOT:PSS, annealing to 180°C and then washed with CLB.

interface layer between the PEDOT:PSS and the BHJ layers that will affect and control the injection and extraction of charge through the anode of the device.

The device study presented here is quite similar to a previous study by of vacuum deposited materials by Tress et. al.[19] In that case, bi-layer OPV devices, fabricated using vacuum processes, were studied and the work functions of the hole transport layer (HTL) and electron transport layer (ETL) were varied. The authors presented a model that explained how the IV curve changed as a function of the energy difference between the Fermi energy of the HTL and the electron donor of the solar cell. They found that lack of alignment between the HTL and HOMO of the donor resulted in S–shaped JV curves.[20] The work function of the HTL layer was varied by changing the doping level.

Our study presents a different challenge because multiple layers or conjugated material cannot normally be deposited using solution methods. The first half of this paper showed that a thin layer (2—5 nm) can be reliably rendered insoluble when deposited and annealed on PEDOT:PSS, which allows us for the first time to ask whether these mixed interface layers are electrically complete and whether they function like the doped HTL layers that were deposited using vacuum techniques by Tress et. al.

Fig. 8 shows JV curves of P3HT/PCBM BHJ devices coated onto interlayers of P3HT, APFO–3, and F8BT formed on PEDOT:PSS by the procedure in Fig. 2. From the UPS and CV data we determine that P3HT is p-type doped by the PSS while

Table 1 Comparison of measurements of energy levels in the polymers P3HT, APFO–3, and F8BT using CV, optical measurements (UV/vis and fluorescence) and ultraviolet photoelectron spectroscopy (UPS). All energy values are scaled to eV's and to the work function (Φ) of PEDOT:PSS with values displayed as the total energy below the vacuum level. Also displayed is whether H_2 is emitted from reaction of PSS with the polymers at 180 °C. 1.

Polymer	**P3HT**	**APFO-3**	**F8BT**
$\mathbf{E}_{ox}$**CV** (V)	0.12	0.87	1.1
$\mathbf{E}_{red}$**CV** (V)	-1.62	-1.52	-1.62
$\mathbf{E}_{HOMO}$**CV** (eV)	4.7	5.45	5.68
$\mathbf{E}_{LUMO}$**CV** (eV)	2.8	3.55	3.38
$\mathbf{E}_{gap}$**CV** (eV)	1.74	2.39	2.72
$\mathbf{E}_{\Delta}$**CV** (eV)	0.4	-0.35	-0.58
$\mathbf{E}_{gap}$**(film - UV/vis)** (eV)	1.92	1.83	2.38
$\mathbf{E}_{gap}$**(liq - UV/vis)** (eV)	2.25	1.94	2.47
$\mathbf{E}_{CT}$**(film - fluor)** (eV)	1.45	1.45	1.75
$\mathbf{E}_{CT}$**(liq - fluor)** (eV)	1.49	1.45	1.81
IE UPS (eV)	4.6	5.3	6.4
EA UPS (eV)	2.1	3.5	3.8
Φ_{ITO} **UPS** (eV)	3.5	2.9*	3.8
$\Phi_{PEDOT:PSS}$**UPS** (eV)	4.2	4.5	4.4
ΔE_F (eV)	-0.7	±0.1*	±0.1
H_2 detected	Yes	No	No
P-type doping	Yes	No	No

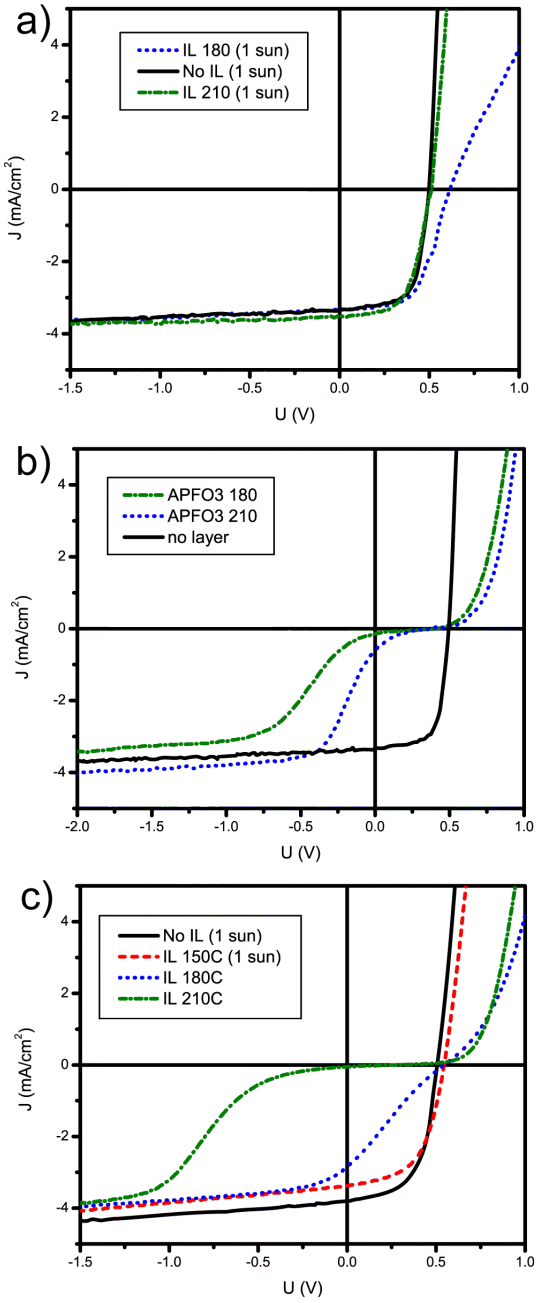

Fig. 8 The current density–voltage curves for P3HT/PCBM OPV devices cast from CLB/NB on interlayers (IL) formed from a) P3HT/PSS, b) APFO–3/PSS and c) F8BT/PSS. All devices are exposed to ∼0.4 suns of simulated sunlight. The black curve in each figure shows a device with no interlayer IL.

APFO–3 and F8BT are not doped by PEDOT:PSS. The P3HT interlayer device has a V_{oc} of 0.55 V and FF of 0.6. The JV curves show the progression of increasing interlayer completeness with BHJ layers cast from a mixture of CLB and NB, a mixture designed to solvent cure the morphlogy of the BHJ layer.[35] CLB/NB cast BHJ devices do not need to be heated and therefore maintain intact interlayers.[35] The device properties were not optimized, but it can be stated that the JV curve is similar to that of a normal P3HT/PCBM OPV device with perhaps reduced V_{oc}. A device with an interlayer of P3HT (already shown to be doped to $P3HT^+$) shows little change when compared to the no interlayer device. This result shows that addition of a 2–5 nm layer of P3HT between the BHJ layer and the PEDOT:PSS has essentially no effect on the J_{sc}, V_{oc}, FF or device PCE. The layer formed at 180 °C shows higher series resistance at higher forward potentials demonstrating that the number of doped paths through the P3HT/PSS interlayer is lower than for the interlayer annealed at 210 °C. A normal annealed BHJ device will have some doped P3HT mixed with PSS, but vertical concentration measurements have shown that in–fact, crystalline domains do not extend to the PEDOT:PSS interface and the PCBM concentration at the interface is still near 50%.[58–61] This comparison shows P3HT/PCBM BHJ mixtures have high PCE under a variety of morphological conditions.[62–64]

The devices fabricated with APFO–3 and F8BT interlayers both show S–shaped JV curves indicating that there is a barrier to extraction of holes through the interlayer. For both device types the temperature at which the interlayer is heated determines the layer thickness. All F8BT is removed with heating to 150 °C while some F8BT enters the interlayer with 180 °C and a full interlayer is formed with annealing to 210 °C. The progression of JV curves can be interpreted as a growing surface coverage of the interlayer polymer with both forward and double diode characteristics in parallel for the incomplete layer formed at 180 °C. We found in working on this system that interlayer formation is highly sensitive to the fabrication conditions. If the P3HT/PCBM BHJ layer was cast from a heated solution (60 °C) onto a complete interlayer, the interlayer displays the characteristics of a mixed interlayer. In addition, if devices with interlayers are heated after the BHJ layer is deposited, the S–shaped characteristic shifts to reflect mixed P3HT/APFO–3 and P3HT/F8BT interlayers. This data shows IV plots with a variety of shapes that have some S–shaped component much like the incomplete interlayers formed at 180 °C, but the data varied widely and so is not shown.

The S–shaped JV curves are modeled using a one dimensional drift–diffusion simulation.[19,65] In this model the BHJ layer is treated as one effective medium. The interlayer is represented as a separate thin layer with a thickness of 3 nm. This value is not measured, but considered as realistic. The metal (-like) contacts PEDOT:PSS and Al are treated with a thermionic model and an injection barrier into the blend of 0.1 eV. The most important input parameters are the effective gap of the blend (1 eV), charge carrier mobilities (μ_e = $6\times^{-4}$ cm^2/Vs, μ_h = $6\times^{-5}$ cm^2/Vs), dielectric constant (3.8), and the effective densities of states (1×10^{19} cm^{-3}, disorder is neglected as it is not important for the conclusions of this study). Recombination is modeled according to Langevin theory with a reduction factor of 0.08. These parameters are in the range of reports from literature.[66–69] It is likely that other parameter combinations would fit the experimental data similarly well. The mobilities and the recombination prefactor were found by fitting the experimental JV–data of devices without interlayer. The mobilities are lower compared to several values reported in literature.[66–70] This is due to a different morphology, as the P3HT:PCBM blend here is much thinner (80 nm) and cast from CLB with a ratio of 3:2 instead of a 1:1 film from oDCB, where optimized thicknesses are in the range of several 100s of nm. The absorbed photon flux that generates charges is derived from the saturated photocurrent at reverse bias and included into a spatially constant generation rate. A constant generation rate is a valid approximation as long as very detailed studies onto the optics of the stack are not done.[71]

To model the JV curves shown in Fig. 9 the material parameters of the blend are maintained. The generation rate is adjusted to reach the saturated photocurrent. Additionally, in case of interlayers, their HOMO is varied to realize the extraction barrier as sketched in Fig. 9b. Drift– and diffusion rates at the barrier are multiplied by a Boltzmann factor. A lowering of the barrier is considered assuming a hopping distance of 1 nm. This approach (details in refs.[19,65]) describes the S–shapes of the JV–curves very well, considering a value for the extraction barrier of 0.4 eV for APFO–3 and 0.52 eV for F8BT. Note that these values are smaller than those expected from the UPS data (cf. Fig. 7). One reason might be that the influence of P3HT:PCBM coated onto the interlayer is not considered in that UPS study. Consequently, dipoles might emerge, which are neglected. Furthermore, disorder might effectively lower the barrier compared to a value derived by the difference of the UPS HOMO onsets. Finally, the unknown interlayer thickness gives rise to uncertainties.

The good coincidence of experimental and simulation data proves that a thin closed interlayer is formed. This interlayer acts as a barrier when extracting photogenerated holes. Presumably, this interlayer is so thin that a tunneling of injection current under forward bias can occur. A tunneling of charges through the interlayer into the blend is not considered in the simulation. Consequently, the simulation underestimates the forward current.

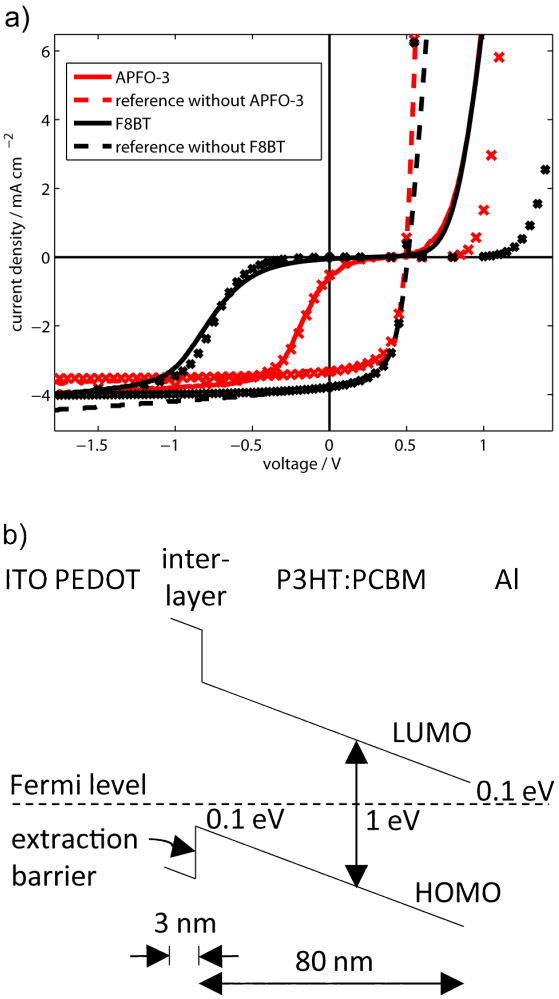

Fig. 9 The current-voltage curves for devices with APFO-3 and F8BT interlayer. The respective reference devices without interlayer are shown as dashed lines. Simulation data are marked with crosses. For devices with interlayer an extraction barrier of 0.4 eV for APFO-3 and 0.52 eV for F8BT is assumed. The inset shows the energy diagram at short circuit used as approximation in the simulation.

4 Conclusions

This article addresses the formation and electrical properties of polymer/PSS mixed interlayers that form at the surface of conjugated polymers with PEDOT:PSS. We first demonstrate that interlayers form upon heating with a wide variety of conjugated polymers. The interlayers have thickness of 2–5 nm, which is limited by the thin PSS layer on top of the PEDOT:PSS. Interlayer polymers can be p–type doped upon mixing with the PSS if their fermi energy is lower than the oxidation potential of the PSS. However insoluble interlayers can form even without the doping reaction. Extensive spectroscopic work shows that doping of the interlayer polymer by PSS has a profound effect on the electronic properties of the interlayer.

Next a series of OPV devices were fabricated on top of prepared interlayers. We show that doped interlayers of P3HT have very litle effect on the JV characteristics. The presence of a skin of P3HT between the PEDOT:PSS and BHJ layer has almost no effect of the JV characteristics which demonstrates that the morphology of P3HT/PCBM is very forgiving and will produce high PCE with a variety of morphology conditions. Mixed interlayers of polymers with higher ionization energy caused higher extraction barriers for holes into the PEDOT:PSS electrode. The extraction barrier is overcome with negative bias and negative bias current density is similar to devices with no interlayer. The JV behavior is predictable based on the Tress model for charge injection and extraction.

5 Acknowledgments

This project was carried out over a period of six years. The salaries of D.L.G., C.W.R., and S.A.M. were supported by the U. S. Department of Energy under Award Number DE-FG36-08GO18018 from 2008–11 and covered device work, contact angle measurements, and XRR. Futher funding from the U. S. Department of Energy, Office of Basic Energy Sciences, Division of Materials Sciences and Engineering, under Award No. DE-SC0010419 covered optical measurements by I.E.J., D.J.B., O.L., continued device work by J.L. and finally writing the paper by A.J.M. in 2013–14. L.A.B. is an Alfred P. Sloan Foundation Fellow. L.A.B. thanks UC Davis for support of this work. Y.Q. and M.-C.J. thank the Okinawa Institute of Science and Technology Graduate University (OIST) for financially supporting the work carried out in OIST. We thank U. Scherf from the University of Wuppertal, Germany and O. Inganas from the University of Linköping, Sweden for donation of APFO–3 samples.

References

1 G. G. Malliaras, *Semiconducting Polymers: Chemistry, Physics and Engineering*, Wiley-VCH, 2006.
2 P. W. M. Blom, V. D. Mihailetchi, L. J. A. Koster and D. E. Markov, *Advanced Materials*, 2007, **19**, 1551–1566.
3 V. I. Arkhipov, E. V. Emelianova, Y. H. Tak and H. Bassler, *Journal of Applied Physics*, 1998, **84**, 848–856.
4 H. Ishii, K. Sugiyama, E. Ito and K. Seki, *Advanced Materials*, 1999, **11**, 605.
5 D. Cahen and A. Kahn, *Advanced Materials*, 2003, **15**, 271–277.
6 S. Kera, Y. Yabuuchi, H. Yamane, H. Setoyama, K. K. Okudaira, A. Kahn and N. Ueno, *Physical Review B*, 2004, **70**, 085304.
7 C. Tengstedt, A. Crispin, C. H. Hsu, C. Zhang, I. D. Parker, W. R. Salaneck and M. Fahman, *Organic Electronics*, 2005, **6**, 21–33.
8 Z. Xu, L. M. Chen, M. H. Chen, G. Li and Y. Yang, *Applied Physics Letters*, 2009, **95**, 013301.
9 G. Heimel, L. Romaner, E. Zojer and J. L. Bredas, *Accounts of Chemical Research*, 2008, **41**, 721–729.
10 P. J. Hotchkiss, S. C. Jones, S. A. Paniagua, A. Sharma, B. Kippelen, N. R. Armstrong and S. R. Marder, *Accounts of Chemical Research*, 2012, **45**, 337–346.
11 T. van Woudenbergh, J. Wildeman and P. W. M. Blom, *Physical Review B*, 2005, **71**, 205216.
12 N. R. Armstrong, P. A. Veneman, E. Ratcliff, D. Placencia and M. Brumbach, *Accounts of Chemical Research*, 2009, **42**, 1748–1757.
13 X. Crispin, V. Geskin, A. Crispin, J. Cornil, R. Lazzaroni, W. R. Salaneck and J. L. Bredas, *Journal of the American Chemical Society*, 2002, **124**, DOI 10.1021/ja025673r—UNSP JA025673R.
14 V. D. Mihailetchi, L. J. A. Koster and P. W. M. Blom, *Applied Physics Letters*, 2004, **85**, 970–972.
15 K. Walzer, B. Maennig, M. Pfeiffer and K. Leo, *Chemical Reviews*, 2007, **107**, 1233–1271.
16 C. D. Muller, A. Falcou, N. Reckefuss, M. Rojahn, V. Wiederhirn, P. Rudati, H. Frohne, O. Nuyken, H. Becker and K. Meerholz, *Nature*, 2003, **421**, 829–833.
17 S. Jungermann, N. Riegel, D. Muller, K. Meerholz and O. Nuyken, *Macromolecules*, 2006, **39**, 8911–8919.
18 A. Kohnen, N. Riegel, J. Kremer, H. Lademann, D. C. Muller and K. Meerholz, *Advanced Materials*, 2009, **21**, 879–+.
19 W. Tress, K. Leo and M. Riede, *Advanced Functional Materials*, 2011, **21**, 2140–2149.
20 A. Kumar, S. Sista and Y. Yang, *Journal of Applied Physics*, 2009, **105**, year.
21 M. Svensson, F. L. Zhang, S. C. Veenstra, W. J. H. Verhees, J. C. Hummelen, J. M. Kroon, O. Inganas and M. R. Andersson, *Advanced Materials*, 2003, **15**, 988–+.
22 S. Kirchmeyer and K. Reuter, *Journal of Materials Chemistry*, 2005, **15**, 2077–2088.
23 A. M. Nardes, M. Kemerink, R. A. J. Janssen, J. A. M. Bastiaansen, N. M. M. Kiggen, B. M. W. Langeveld, A. J. J. V. van Breemen and M. M. deKok, *Advanced Materials*, 2007, **19**, 1196–1200.
24 K. Z. Xing, M. Fahlman, X. W. Chen, O. Inganas and W. R. Salaneck, *Synthetic Metals*, 1997, **89**, 161–165.
25 G. Greczynski, T. Kugler and W. R. Salaneck, *Thin Solid Films*, 1999, **354**, 129–135.
26 G. Greczynski, T. Kugler, M. Keil, W. Osikowicz, M. Fahlman and W. R. Salaneck, *Journal of Electron Spectroscopy and Related Phenomena*, 2001, **121**, 1–17.
27 X. Crispin, S. Marciniak, W. Osikowicz, G. Zotti, A. W. D. Van der Gon, F. Louwet, M. Fahlman, L. Groenendaal, F. De Schryver and W. R. Salaneck, *Journal of Polymer Science Part B-Polymer Physics*, 2003, **41**, 2561–2583.
28 X. Crispin, F. L. E. Jakobsson, A. Crispin, P. C. M. Grim, P. Andersson, A. Volodin, C. van Haesendonck, M. Van der Auweraer, W. R. Salaneck and M. Berggren, *Chemistry of Materials*, 2006, **18**, 4354–4360.
29 D. M. Huang, S. A. Mauger, S. Friedrich, S. J. George, D. Dumitriu-LaGrange, S. Yoon and A. J. Moule, *Advanced Functional Materials*, 2011, **21**, 1657–1665.
30 L. A. A. Pettersson, T. Johansson, F. Carlsson, H. Arwin and O. Inganas, *Synthetic Metals*, 1999, **101**, 198–199.
31 T. Johansson, L. A. A. Pettersson and O. Inganas, *Synthetic Metals*, 2002, **129**, 269–274.
32 A. M. Nardes, M. Kemerink and R. A. J. Janssen, *Physical Review B (Condensed Matter and Materials Physics)*, 2007, **76**, 085208–7.
33 A. M. Nardes, M. Kemerink, M. M. de Kok, E. Vinken, K. Maturova and R. A. J. Janssen, *Organic Electronics*, 2008, **9**, 727–734.
34 S. A. Mauger, L. Chang, C. W. Rochester and A. J. Moulë, *Organic Electronics*, 2012, **13**, 2747–2756.
35 A. J. Moulé and K. Meerholz, *Advanced Materials*, 2008, **20**, 240–245.
36 A. B. D. Cassie and S. Baxter, *Transactions of the Faraday Society*, 1944, **40**, 546–551.
37 Y. Kim, A. M. Ballantyne, J. Nelson and D. D. C. Bradley, *Organic Electronics*, 2009, **10**, 205–209.
38 D. Chen, A. Nakahara, D. Wei, D. Nordlund and T. P. Russell, *Nano Letters*, 2010, **11**, 561–567.
39 C. Ton-That, A. G. Shard and R. H. Bradley, *Langmuir*, 2000, **16**, 2281–2284.
40 S. Doniach and Šunjić, *Journal of Physics C*, 1970, **3**, 285.
41 D. A. Shirley, *Physical Review B*, 1972, **5**, 4709.
42 P. E. S. J. F. Moulder, W. F. Stickle and K. D. Bomben, *Handbook of X-ray Photoelectron Spectroscopy*, Physical Electronics, 1995.
43 J. Hwang, F. Amy and A. Kahn, *Organic Electronics*, 2006, **7**, 387–396.
44 A. Köhnen, M. Brücher, A. Reckmann, H. Klesper, A. von Bohlen, R. Wagner, A. Herdt, D. Lützenkirchen-Hecht, R. Hergenröader and K. Meerholz, *Macromolecules*, 2012, **45**, 3487–3495.
45 M. Fahlman, A. Crispin, X. Crispin, S. K. M. Henze, M. P. d. Jong, W. Osikowicz, C. Tengstedt and W. R. Salaneck, *Journal of Physics: Condensed Matter*, 2007, 183202.
46 H. Frohne, S. E. Shaheen, C. J. Brabec, D. C. Muller, N. S. Sariciftci and K. Meerholz, *Chemphyschem*, 2002, **3**, 795–799.
47 S. Braun, M. P. de Jong, W. Osikowicz and W. R. Salaneck, *Applied Physics Letters*, 2007, **91**, 3.
48 M. M. Bouman, E. E. Havinga, R. A. J. Janssen and E. W. Meijer, *Molecular Crystals and Liquid Crystals Science and Technology Section a-Molecular Crystals and Liquid Crystals*, 1994, **256**, 439–448.
49 M. A. Stevens, C. Silva, D. M. Russell and R. H. Friend, *Physical Review B*, 2001, **16**, 165213.
50 C. Brabec, V. Dyakonov, J. Parisi and N. S. Sariciftci, *Organic Photovoltaics*, Springer, Berlin, Heidelberg, New York, 2003, p. 295.
51 W. R. Salaneck, K. Seki, A. Kahn and J.-J. Pireaux, *Conjugated Polymer And Molecular Interfaces: Science And Technology For Photonic And Optoelectronic Application*, CRC Press, 2001.
52 Z.-L. Guan, J. B. Kim, H. Wang, C. Jaye, D. A. Fischer, Y.-L. Loo and A. Kahn, *Organic Electronics*, 2010, **11**, 1779–1785.
53 S. K. M. Jonsson, E. Carlegrim, F. Zhang, W. R. Salaneck and M. Fahlman, *Japanese Journal of Applied Physics*, 2005, **44**, 3695–3701.
54 J. Zaumseil, C. L. Donley, J.-S. Kim, R. H. Friend and H. Sirringhaus, *Advanced Materials*, 2006, **18**, 2708–2712.
55 J. Zaumseil and H. Sirringhaus, *Chemical Reviews*, 2007, **107**, 1296–1323.
56 Y. Zhang and P. W. M. Blom, *Applied Physics Letters*, 2011, **98**, 143504.
57 M. T. Greiner, M. G. Helander, W.-M. Tang, Z.-B. Wang, J. Qui and L. Z.-H., *Nature Materials*, 2012, **11**, 76.
58 S. A. Mauger, L. L. Chang, S. Friedrich, C. W. Rochester, D. M. Huang,

P. Wang and A. J. Moulé, *Advanced Functional Materials*, 2013, **23**, 1935–1946.
59 J. D. Roehling, K. J. Batenburg, F. B. Swain, A. J. Moule and I. Arslan, *Advanced Functional Materials*, 2013, **23**, 2115–2122.
60 O. Wodo, J. D. Roehling, A. J. Moulé and B. Ganapathysubramanian, *Energy & Environmental Science*, 2013, **6**, 3060–3070.
61 J. D. Roehling, C. W. Rochester, H. W. Ro, P. Wang, J. Majewski, K. J. Batenburg, I. Arslan, D. M. Delongchamp and A. J. Moulé, *Journal of Polymer Science B: Polymer Physics*, 2014, **52**, 1290–1300.
62 A. J. Moulé and K. Meerholz, *Advanced Functional Materials*, 2009, **19**, 3028–3036.
63 S. V. Kesava, R. Dhanker, D. R. Kozub, K. Vakhshouri, U. H. Choi, R. H. Colby, C. Wang, A. Hexemer, N. C. Giebink and E. D. Gomez, *Chemistry of Materials*, 2013, **25**, 2812–2818.
64 F. C. Krebs, J. Fyenbo, D. M. Tanenbaum, S. A. Gevorgyan, R. Andriessen, B. van Remoortere, Y. Galagan and M. Jorgensen, *Energy & Environmental Science*, 2011, **4**, 4116–4123.
65 W. Tress, *Organic Solar Cells*, Springer, 2014.
66 R. H ausermann, E. Knapp, M. Moos, N. A. Reinke, T. Flatz and B. Ruhstaller, *Journal of Applied Physics*, 2009, **106**, 104507.
67 N. S. Christ, S. W. Kettlitz, S. Valouch, S. Zfle, C. Grtner, M. Punke and U. Lemmer, *Journal of Applied Physics*, 2009, **105**, 104513.
68 L. J. A. Koster, V. D. Mihailetchi and P. W. M. Blom, *Applied Physics Letters*, 2006, **88**, 093511.
69 K. Maturova, S. S. van Bavel, M. M. Wienk, R. A. J. Janssen and M. Kemerink, *Advanced Functional Materials*, 2011, **21**, 261–269.
70 V. D. Mihailetchi, H. X. Xie, B. de Boer, L. J. A. Koster and P. W. M. Blom, *Advanced Functional Materials*, 2006, **16**, 699–708.
71 W. Tress, A. Merten, M. Furno, M. Hein, K. Leo and M. Riede, *Advanced Energy Materials*, 2013, **3**, 631–638.